ISSN NO: 0776-3808

Fabrication of bare and Cobalt doped $PbMoO_4$ Nanoparticles: Enhanced photocatalytic activity under visible light irradiation

Akilandeswari. S[1], Niranjana. M[2], Rajesh. G[3]
[1]*PG & Research Department of Physics, Government College for Women (Autonomous), Kumbakonam, Tamil Nadu 612 001, India.*
[2]*Department of Physics, Annamalai University, Annamalai Nagar, Chidambaram, Tamil Nadu 608 002, India.*
[3]*Department of Chemical Engineering, Sri Sivasubramaniya Nadar College of Engineering, Tamil Nadu 603 001, India.*

[1]akilaphy2010@gmail.com,[2]niranjana29071997@gmail.com, [3]rajeshgk20@gmail.com

Abstract

Enhancing the photocatalytic activity through doping ions has garnered significant research interest. In this research, bare and Co-doped $PbMoO_4$ nanoparticles were successfully prepared by using co-precipitation technique to improve the degradation performance of organic pollutants under visible light irradiation. The structural, morphological, optical and photoluminescence properties of the synthesized nanoparticles were examined using XRD, SEM-EDS, HRTEM with SEAD, UV-DRS and PL spectroscopy. Differential Reflectance Spectroscopy (DRS) results revealed a smaller band gap for Co (0.05 M) doped $PbMoO_4$ nanoparticles compared to bare $PbMoO_4$. In particular, Co (0.05 M) doped $PbMoO_4$ catalyst demonstrated 88% removal of Brilliant Blue (BB) and 94% removal of Brilliant Green (BG) dyes under visible light irradiation within 120 minutes, this catalyst showed recyclability under optimized conditions. Free radical experiments indicated the involvement of $^{\bullet}OH$ and h^+ radicals in the degradation of BB and BG dyes, while Chemical Oxygen Demand measurement confirmed the complete mineralization of both dye molecules. This work provides valuable insights into the efficient degradation of organic pollutants by doping metal ions in semiconductor photocatalysts.

Keywords: **Co-$PbMoO_4$, Brilliant blue and Brilliant green, Photocatalytic application, Reusability**

I. INTRODUCTION

The escalation of global industrialization triggers major environmental pollution issues, primarily due to the substantial water consumption and discharge of untreated organic pollutants by industrial sectors. Wastewater from textile, paper, paint, leather and other industries contains non-biodegradable residual dyes, posing a significant challenge for pollution control and elimination [1], [2]. Organic dyes emerge as the primary pollutants in wastewater. The inadequate treatment of discharged pollutants leads to sever health risks for humans and ecosystems alike [3]. In response to these challenges, researchers are directed their efforts towards photocatalysis is an ideal purification technique for removing organic pollutants [4]. Semiconductor-based photocatalysts, in particular, have gained significant attention to their potential in environmental remediation. This includes the effective removal of industrial waste as well as process like water splitting into H_2 and O_2, which are critical for preventing environmental problems [5].

Metal molybdate have attracted significant interest for their diverse applications across various technological domains, including photocatalytic, optics, magnetism, gas sensors, antibacterial, and electrochemical capabilities [6]. There are several visible light based dissimilar semiconductor oxide materials applied for photocatalytic degradation including $MgMoO_4$ [7], $SrMoO_4$ [8], $ZnMoO_4$ [9], $NiMoO_4$ [10], $CaMoO_4$ [11], $PbMoO_4$ [12], $BaMoO_4$ [13]. Among these, Lead molybdate ($PbMoO_4$) is a most attractive p-type semiconductor material. Various methods have been employed to obtain $PbMoO_4$, including microwave irradiation, hydrothermal, sonochemical, co-precipitation, and solvothermal techniques [14-17], etc. Among these, co-precipitation method stands out for its simplicity, low cost, and ease to synthesis. It has garnered special attention for its ability to produce oxides with high crystallinity, which facilitates easy dispersion in aqueous media, reduces reaction times, lower synthesis temperatures,

ISSN NO: 0776-3808

allows precise control over reaction parameters, and enables manipulation of product size and morphology. This ultimately leads to enhanced product purity and material properties [18], [19].

The recent focus on doping atoms into semiconductor materials has emerged because of its potential to enhance photocatalytic activity. Doping metal ions semiconductor particles offers several advantages, including the dopant's temporary trapping of photogenerated charge carriers and the prevention of their recombination during displacement from the material's interior to the surface. Additionally, it enhances the association of functionalized organic pollutants with doping ion surface sites [17]. Doping with Gd [4], Ag [20], Eu [21], Co [22], Tb [23], and Ln [24] ions is a highly effective method to improve the photoluminescence and photocatalytic performance of $PbMoO_4$. Cobalt doping due to the favorable size compatibility between Co^{2+} (CN = 4) and Mo^{6+} (CN = 4) compared to Pb^{2+} (CN =8), which increases the likelihood of Co^{2+} occupying Mo^{6+} sites with a coordination number (CN) of 4 [25]. Cobalt (Co) is recognized as one of the most effective dopants. By introducing doped Co ions into semiconductors, it creates Co impurity energy levels, which serve to decrease the band gap. Which improves the material capacity for charge separation and transport within the material [26].

In the present work, fabrication of $PbMoO_4$ material with different concentrations of Co (0.025, 0.050, 0.075 M) ions by co-precipitation route were carried out. The extensive investigation of the structural, morphological, optical properties of the synthesized nanoparticles, and evaluated their photodegradation performances by degradation BG and BB dyes were dispersed. Notably, Co (0.050 M) doped $PbMoO_4$ nanoparticles exhibited superior photocatalytic efficiencies for the degradation of BG (94%) and (88%) dyes within 120 min under visible light irradiation. In addition, Co (0.050 M) doped $PbMoO_4$ nanoparticles were easily recovered and demonstrated reasonable stability after five consecutive runs. The findings suggest that Co-doped $PbMoO_4$, particularly at 0.05 M cobalt concentration, are effective catalysts for removing harmful contaminants under visible light, with promising applications in surface cleaning and various energy-related fields.

II. Materials and Methods

A. Materials

All chemical substances used in the preparation process, such as Cobalt (II) nitrate hexahydrate ($Co(NO_3)_2.2H_2O$), Lead nitrate ($Pb(NO_3)_2$), Sodium molybdate ($Na_2.MoO_4.2H_2O$), Brilliant green ($C_{27}H_{34}N_2O_4S$) and Brilliant blue ($C_{37}H_{34}N_2Na_2O_9S_3$) were purchased from Merck and SD chemicals. All the chemical reagents (AR grade) were used without any further processing. Ethanol and ultrapure water were utilized for the dilution and sample preparation processes.

B. Synthesis of bare and Co (0.025-0.075 M) doped $PbMoO_4$ nanoparticles

The bare and Co (0.025, 0.050, 0.075 M) doped $PbMoO_4$ nanoparticles were synthesized using the co-precipitation method. Initially, 4.96 g of Lead nitrate was dispersed in 50 ml of ultrapure water and stirred continuously for 15 minutes to achieve a homogeneous suspension. Similarly, a specific amount of Cobalt (II) nitrate hexahydrate was dispersed in another 50 ml of ultrapure water and added to the above mixture, followed by an additional 30 minutes of stirring. Then, 6.04 g of Sodium molybdate was dispersed in 50 ml of ultrapure water, and this solution was slowly added to the previous mixtures while being vigorously stirring. The resulting mixtures were then stirred magnetically for 5 h at 80^{o}C. Subsequently, the resulting precipitate was filtered and washed repeatedly with ultrapure water and ethanol separately. The collected precipitate was, then dried for 5 h at 100^{o}C and subsequently calcined for 4 h at 700^{o}C. A similar procedure was followed to synthesize the bare nanoparticles.

C. Characterizations

The crystallinity of the synthesized bare and doped $PbMoO_4$ samples was characterized using X-ray diffraction (XRD) with Cu Kα incident radiation (λ = 0.15406 nm) on a Shimadzu XRD-6000, operated at 40 kV and 30 mA. The UV-DRS spectra of all prepared sample were analyzed using a UV-2600 series spectrophotometer in reflectance mode. The PL spectra were recorded with a Perkin Elmer fluorescence spectrophotometer, model: LS 45 covering the range from 200 nm to 900 nm. The morphological characterization of the bare and Co-doped $PbMoO_4$ nanoparticles was conducted using a SEM (JEOL-JSM-

IT 200). The micrographs and average nanoparticle size were obtained by using HRTEM (JEOL JAPAN, JEM-2100 plus).

D. Photocatalytic measurements

The Co (0.050 M) doped $PbMoO_4$ photocatalyst was employed for the degradation of BG and BB dyes under visible light irradiation. The experiments were conducted in a visible light reactor. 150 ml of BG and BB dye aqueous solutions (Initial concentration: $3x10^{-5}$ M) was taken in a separate beaker. To this 8 mg of (0.05 M) Co doped $PbMoO_4$ catalyst is added and whole mixture was magnetic stirred in the dark room for 30 minutes to establish adsorption-desorption equilibrium before the reaction. The suspension was then stirred under visible light, and 5 ml of the reacted suspension was collected at specified intervals. The catalyst was separated by centrifugation at 3500 rpm. The concentrations of BB and BG were measured at wavelengths of 308, 583 nm and 426, 624 nm using UV-Vis spectroscopy. The degradation efficiency was determined using the following equation,

$$D = \frac{C_0 - C_t}{C_0} \times 100\ \% \quad (1)$$

Where C_0 is the initial and C_t is the dye concentration at a certain irradiation time (t) of both BB and BG dyes.

III. Results and Discussion

A. X-Ray diffraction analysis (XRD)

The diffraction pattern depicted in Fig. 1 reveals the distinctions between $PbMoO_4$ and Co (0.025, 0.050, 0.075 M) doped $PbMoO_4$ nanoparticles. Across all sample, the peak intensities and positions at 18, 27, 29, 33, 37, 40, 43, 44, 47, 51, 55, 56, 71, 72, 75, 76 and 78° consistently match with the (101), (112), (004), (200), (114), (105), (123), (204), (220), (116), (312), (224), (208), (316), (332), (404) and (420) planes, which are well matched with the $PbMoO_4$ system (JCPDS no: 44-1486) [4]. Therefore, the results indicated that cobalt doping did not cause any significant changes in the $PbMoO_4$ host lattice or introduce any new phases. This may be reasonable for the addition of Co (0.74 Å), by Pb (1.19 Å), Mo (0.65Å) of greater ionic radius. The crystallite size (*D*) of both bare and Co (0.025, 0.05, 0.075 M) doped $PbMoO_4$ nanoparticles were determined by Scherrer's equation [27],

$$D = \frac{K\lambda}{\beta \cos\theta} \quad (Å) \quad (2)$$

Here, D represents the crystalline size, k is the constant related to the crystallite shape (k = 0.9), λ denotes the wavelength of radiation, β stands for the FWHM, and θ refers to the Bragg's reflection angle. The crystallite sizes show slight variations, both increasing and decreasing, with changes in cobalt concentration (0.025, 0.050 and 0.075 M), and the observed values for all samples are detailed in Table I.

TABLE I

THE CRYSTALLITE SIZE, PHASES AND ENERGY GAP OF BARE AND COBALT (0.025, 0.050, 0.075 M) DOPED $PbMoO_4$

S. No.	Materials	Crystallite size (nm)	Phases	Energy gap (eV)
1.	$PbMoO_4$	19.12	Tetragonal	3.12
2.	$PbMoO_4$: Co (0.025 M)	20.70	Tetragonal	2.94
3.	$PbMoO_4$: Co (0.050 M)	21.71	Tetragonal	2.76
4.	$PbMoO_4$: Co (0.075 M)	20.94	Tetragonal	2.89

ISSN NO: 0776-3808

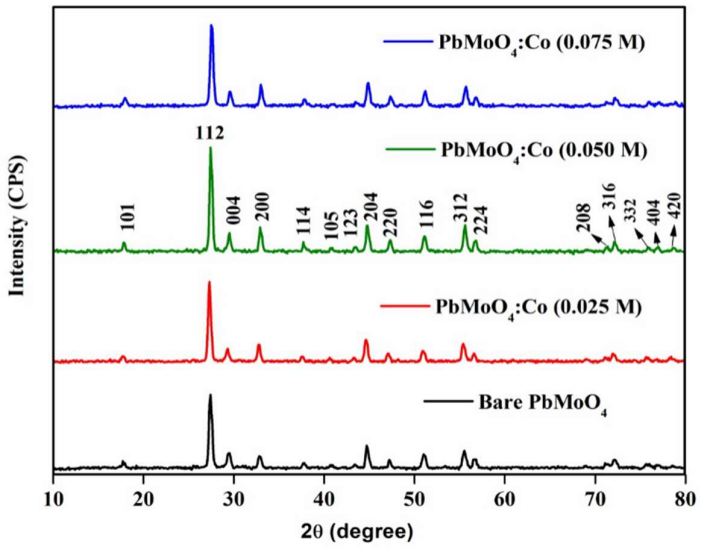

Fig. 1 XRD pattern of bare $PbMoO_4$ and Co (0.025, 0.05, 0.075 M) doped $PbMoO_4$ nanoparticles

B. UV-Vis DRS analysis

Utilizing DRS is crucial for analyzing the band structure of metal oxide nanomaterials. Fig. 2a and 2b show the absorption spectra and energy gaps for both bare and Co (0.025, 0.05, 0.075 M) doped $PbMoO_4$ nanoparticles. It is observed that all samples, including $PbMoO_4$ and Co doped $PbMoO_4$, exhibit a broad absorption band covering from UV to visible wavelengths, as shown in Fig. 2a. In the case of Co doped samples, there is a slight shift of the optical absorption across a wide range, particularly in the visible spectrum. The energy gap (E_g) of a bare and Co (0.025-0.075) doped $PbMoO_4$ can be determined using equation 3 as follows [29]:

$$\alpha = \frac{A(h\nu - E_g)^{1/2}}{h\nu} \tag{3}$$

Here, α represents absorbance, A is the proportionality constant, ν denotes frequency, h stands for Planck's constant, and E_g signifies the optical band gap. The band gap was calculated by extrapolating the linear portion of the plot of $[F(R).h\nu]^2$ vs (hν) [28]. Notably, the band gap energies of Co doped $PbMoO_4$ nanoparticles decreased significantly with increasing cobalt concentration, as detailed in Table I.

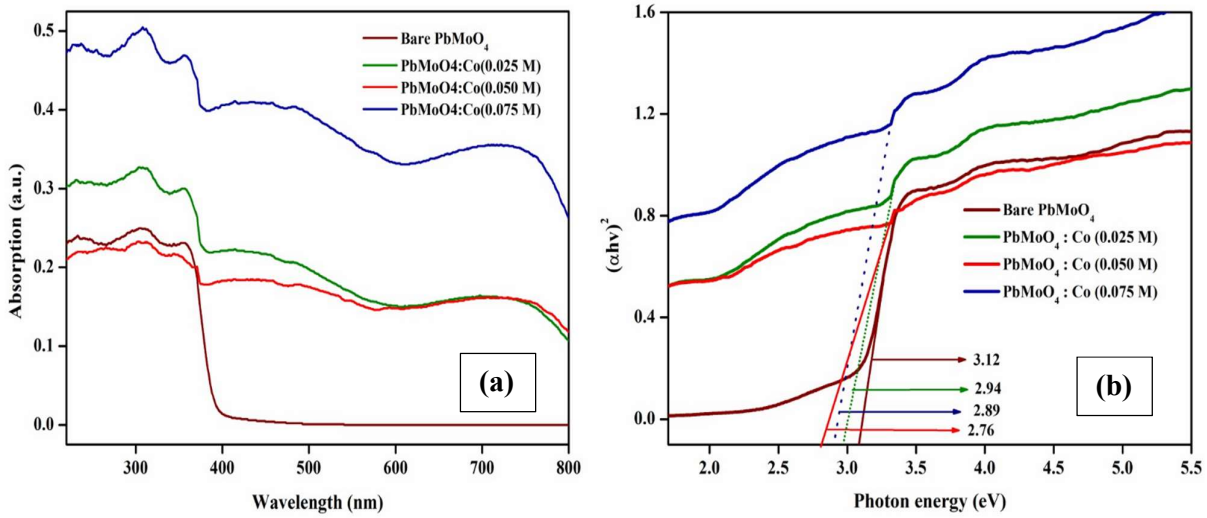

Fig. 2 UV-DRS Absorption (a) and Energy gaps (b) of bare and Co (0.025, 0.050, 0.075 M) doped $PbMoO_4$ nanoparticles

ISSN NO: 0776-3808

Fig. 2b shows that the band gap energy of bare $PbMoO_4$ nanoparticles was 3.12 eV, which decreased to 2.94, 2.76 and 2.89 eV with increasing cobalt doping, respectively. The sample displays a broad absorption range from 250 to 400 nm, attributed to O-Mo charge transfer electronic transitions. The band gap in the materials is related with absorbance and photon energy. Consequently, combining absorbance and PL measurements helps explore the energy levels within the materials and determine the optical band gap value.

C. SEM analysis

The SEM analysis elucidated the morphology characteristics of the optimized Co (0.050 M) doped $PbMoO_4$ nanoparticles. As depicted in Fig. 3a-c, the Co (0.050 M) doped $PbMoO_4$ nanoparticles displayed spherical structures with little agglomeration at different magnifications. Additionally, it was observed that there was no substantial difference in the size and shape of their morphology. EDS analysis is used to study the elemental conformation of the Co (0.050 M) doped $PbMoO_4$ nanoparticles. The presence of Pb, Mo, Co and O peaks without any impurities is confirmed from Fig. 3d.

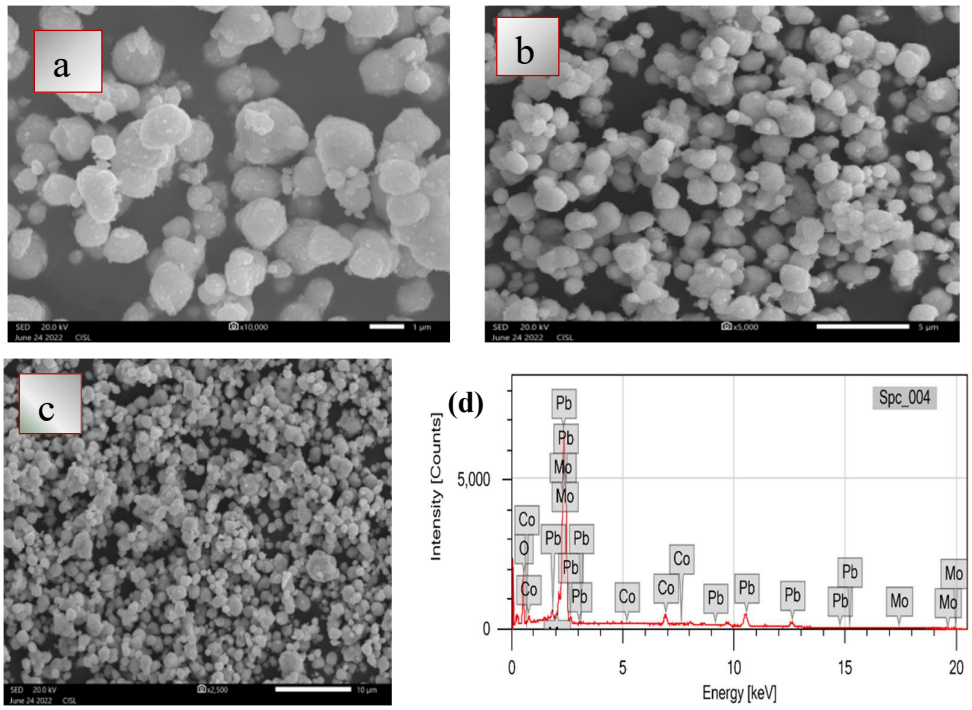

Fig. 3 (a, b, c) SEM images of Co (0.050 M) doped $PbMoO_4$ nanoparticles with different magnifications and (d) EDS analysis of Co (0.050 M) doped $PbMoO_4$ nanoparticles

D. HRTEM analysis

HRTEM analysis can be used to analyze the microstructure and the interface composition of Co (0.050 M) doped $PbMoO_4$ nanoparticles. Fig. 4(a-c) depicts TEM images of Co (0.050 M) doped $PbMoO_4$ at different magnifications and it depicts particles that are mostly spherical particles with little agglomeration. Also, clear lattice spacing could be seen in the HRTEM analysis, as shown in Fig. 4d. The observed lattice fringes of 0.327 nm were in line with the (112) planes, showing that the $PbMoO_4$ crystal structure is tetrahedral. In this, results confirmed the absence of any other impurities in the product. Moreover, the SAED pattern exhibited concentric rings and bright spots, confirming the polycrystalline nature of the Co (0.050 M) doped $PbMoO_4$, as illustrated in Fig. 4e. The particle size, determined to be 23.05 nm for Co (0.050 M) doped $PbMoO_4$ nanoparticles, was derived from histogram results, as illustrated in Fig. 4f.

ISSN NO: 0776-3808

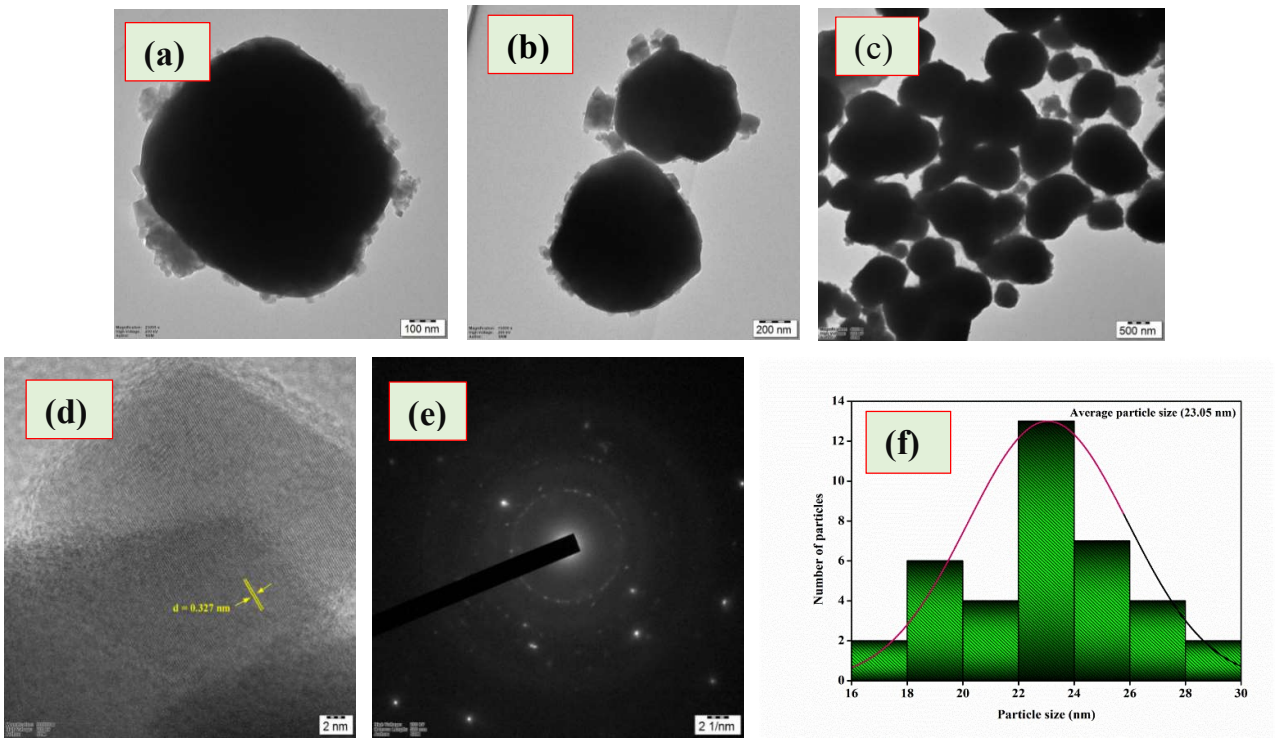

Fig. 4 HRTEM images of Co (0.050 M) doped $PbMoO_4$ nanoparticles (a-c), lattice fringes (d), SEAD pattern (e) and Histogram (f)

E. Photoluminescence spectroscopy (PL)

Photoluminescence spectroscopy proves to be an effective method for assessing the electronic structure, presence of oxygen vacancies, surface defects, charge carrier separation and recombination in both bare and Co (0.025, 0.050, 0.075 M) doped $PbMoO_4$ nanoparticles. The PL spectrum of the prepared nanoparticles was obtained using excitation lines at 257, 309 and 356 nm, as shown in Fig. 5. The resulting spectra exhibit one strong and three weak peaks at 608, 340, 455 and 479 nm, respectively, indicating emission peaks corresponding to blue and green wavelengths, consistent with previous studies [30]. The PL spectrum displays a broad band across the visible range from 320 to 650 nm, with a dominant peak at 608 nm corresponding to orange emission [12]. Notably, the spectrum also shows characteristic blue emission peak around 455, 479 nm, attributed to charge transfer transitions within the MoO_4 clusters. Additionally, a weak green emission band at 550 nm suggests the presence of Frenkel defects (where an oxygen ion moves to an interstitial position, creating a vacancy) in the surface layers of the $PbMoO_4$. These findings indicate that the luminescence properties of $PbMoO_4$ are highly sensitive to its structure and significantly influenced by structural defects [21].

The intense PL peaks suggest rapid recombination of photoinduced carriers, which may result in lower photocatalytic efficiency [31]. It is well-documented that broad PL spectra indicate the involvement of multiple energy states within the band gap, capable of trapping electrons during excitation and emission processes. Electronic transitions within the MoO_4 tetrahedral groups are responsible for the observed blue PL emission in molybdates. This blue emission arises from isolated transitions of MoO_4^{2-} group, while the green emission results from the overlap of two bands. This overlap involves the transfer of an electron from an orbital primarily associated with Pb^{2+} to a vacant orbital of a MoO_4^{2-} group, mainly characterized by d-orbitals. Variations in particle size distribution, degree of crystallinity, morphology and surface defects may also play a vital role [32], [33].

ISSN NO: 0776-3808

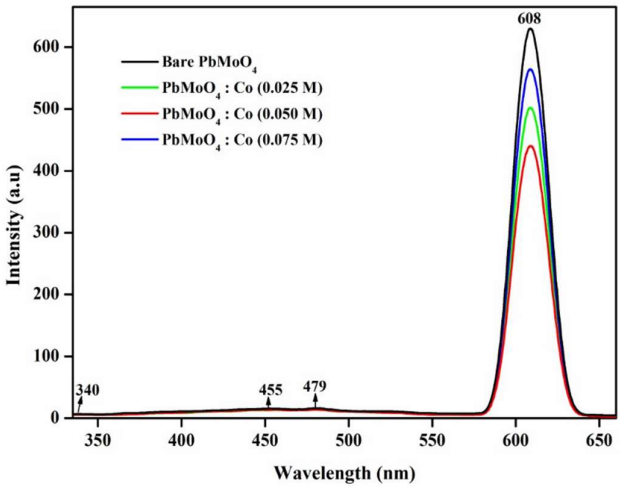

Fig. 5 PL emission spectra of bare $PbMoO_4$ and Co (0.025, 0.050, 0.075 M) doped $PbMoO_4$ nanoparticles

F. Photocatalytic activity

The photocatalytic activities of Co (0.050 M) doped $PbMoO_4$ Products were evaluated for the removal of two different dyes (BB and BG) under visible light irradiation. Fig. 6a and 6b depicts the strong broad and slightly weaker absorption peaks at 583, 308 nm for BB dye and 624, 426, 318 nm for BG dye solutions in the Co (0.05 M) doped $PbMoO_4$ catalyst. As the degradation process progressed, the intensity of the main absorption peaks for BB and BG dye solutions gradually decreased. Bare $PbMoO_4$, Co (0.025 and 0.075) doped $PbMoO_4$ were also used to degrade BB and BG dye under identical conditions, achieving degradation efficiencies of 41%, 85%, 79%, for BB and 49%, 87%, 83% for BG, respectively (not shown). This decrease can be attributed to the generation of e^- - h^+ pairs, leading to gradual reduction in the concentration of Co (0.050 M) doped $PbMoO_4$ nanoparticles in the aqueous solution [26], [34]–[37].

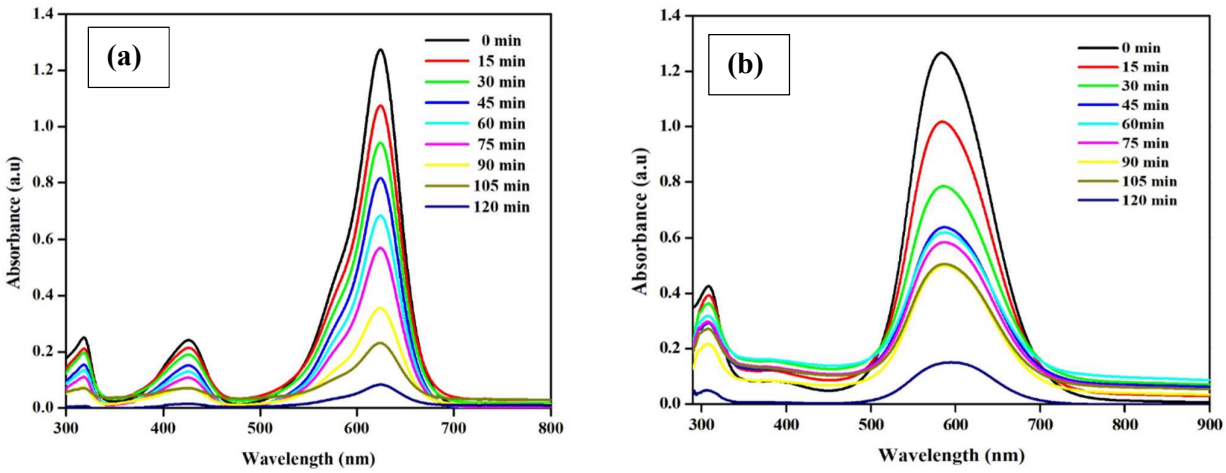

Fig. 6 Absorption spectra of BG dye (a) and BB dye (b) solutions displaying photocatalytic degradation using Co (0.050 M) doped $PbMoO_4$ nanoparticles

ISSN NO: 0776-3808

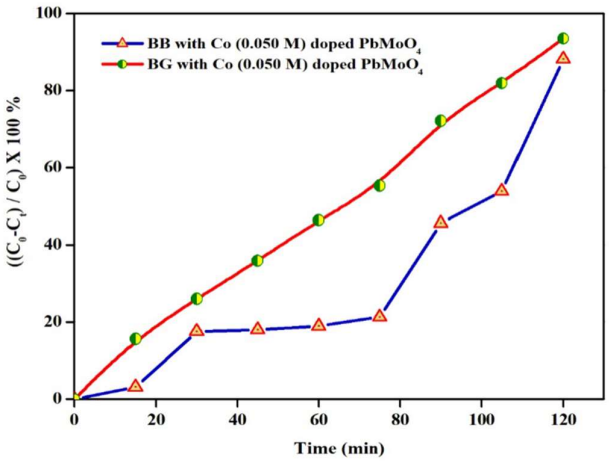

Fig. 7 Plot of degradation efficiency versus time for BB and BG dyes using Co (0.050 M) doped $PbMoO_4$ nanoparticles

G. COD analysis

COD analysis is an essential method for identifying organic contaminants in water bodies. In this study, COD analysis was performed on BG and BB dyes following the photodegradation process, revealing complete mineralization of organic substances within 120 minutes of illumination. The photodegradation rates of BG and BB dyes reached approximately 94% and 88% respectively as shown in fig. 7. Additionally, COD experiments were conducted on Co (0.050 M) doped $PbMoO_4$ for BG and BB dyes under optimal conditions. The COD degradation rates for BG and BB were 89% and 79% respectively. With the photocatalyst under visible irradiation for 120 miniutes indicating complete mineralization of the organic substances into CO_2 and H_2O. The COD removal rates of BG and BB dyes at specific time intervals are mentioned in Table II.

TABLE II

PERCENTAGE COD REDUCTION OF BB AND BG SUBSTANCES USING Co (0.050 M) DOPED $PbMoO_4$

S. No.	Time (min)	% COD removal for BB dye: Co (0.050 M) doped $PbMoO_4$	% COD removal for BG dye: Co (0.050 M) doped $PbMoO_4$
1	15	20	33
2	30	27	58
3	45	57	66
4	60	62	70
5	75	63	76
6	90	75	79
7	105	77	83
8	120	79	89

H. Photodegradation mechanism

Figure 8 illustrates the photocatalytic mechanism for the degradation of BG and BB dyes. The generation of photoinduced electron-hole pairs is influenced by the optical band gap. This process is less effective in bare $PbMoO_4$ nanoparticles due to their wide band gap, which is mainly activated in the UV region. In contrast, narrowing the energy gap enhances the production of photogenerated charge carriers. DRS analysis indicates a significant reduction in the band gap of $PbMoO_4$ and Co doped $PbMoO_4$ from 3.12 eV to 2.76 eV, leading to a higher density of e^- and h^+ pairs available for photocatalytic reactions. Cobalt ions doping introduces additional defects and oxygen vacancies into the $PbMoO_4$ matrix, improving absorption in the visible range and thereby enhancing degradation activity. The movement of charge carriers on the

ISSN NO: 0776-3808

photocatalysts surface, interact with the surface adsorbed hydroxyl groups and oxygen molecules, which initiates a rapid degradation process. Excited electrons with strong reducing power react with adsorbed oxygen molecules to generate superoxide radical anions ($^{\bullet}O_2^-$), reducing e^-- h^+ recombination. Likewise, photo-generated holes with strong oxidizing power interact with surface hydroxyl groups to produce highly reactive hydroxyl radicals ($^{\bullet}OH$) [38]–[40]. The photodegradation process of BG and BB is described by Eqs. 4-9:

$$\text{Co-PbMoO}_4 + h\nu \rightarrow \text{Co-PbMoO}_4\,(e_{CB}^- + h_{VB}^+) \quad (4)$$

$$e_{CB}^- + O_2 \rightarrow {}^{\bullet}O_2^- \quad (5)$$

$$h_{VB}^+ + H_2O \text{ (or OH)} \rightarrow H^+ + {}^{\bullet}OH^- \quad (6)$$

$$h_{VB}^+ + OH^- \rightarrow {}^{\bullet}OH \quad (7)$$

$$^{\bullet}OH^- + \text{(BG and BB) dyes} \rightarrow \text{Degradation products } (H_2O + CO_2) \quad (8)$$

$$^{\bullet}O_2^- + \text{(BG and BB) dyes} \rightarrow \text{Degradation products } (H_2O + CO_2) \quad (9)$$

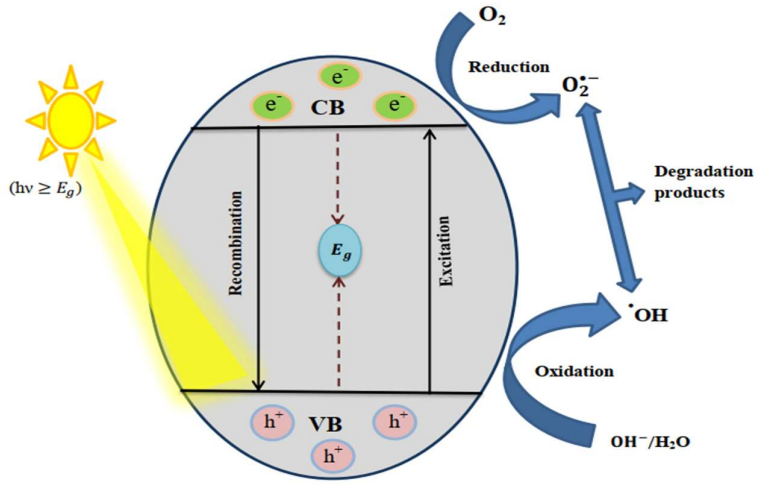

Fig. 8 Schematic representation of the photocatalysis mechanism in a Co (0.050 M) doped $PbMoO_4$ sample

I. Recyclability

To assess the stability and recyclability of the optimized Co (0.05 M) doped $PbMoO_4$ sample the photocatalyst was enhanced, filtered and dried for reuse. The photocatalytic degradation process involved investigating the collective reactant-catalyst interaction for recyclability, demonstrating stable and reusable performance over 5 repetitive cycles. Table III illustrates the degradation efficiency of Co (0.05 M) doped $PbMoO_4$ for Brilliant Blue (BB) and Brilliant Green (BG) dyes across five consecutive runs. The result indicates that the Co (0.05 M) doped $PbMoO_4$ exhibits good mechanical stability and reusability.

TABLE III

REUSABILITY OF Co (0.050 M) DOPED $PbMoO_4$ CATALYST WITH BB AND BG DYE DEGRADATION

S. No.	Number of cycles	Degradation % for BB dye	Degradation % for BB dye
1	1	88	94
2	2	87	92
3	3	85	91
4	4	84	89
5	5	83	85

ISSN NO: 0776-3808

J. Determination of Active Radicals

The trapping experiments revealed the main active species involved in the Co (0.050 M) doped $PbMoO_4$ photocatalytic reactions system. Four different scavengers namely Tetrabutylammonium hydroxide (TBAH), Sodium fluoride (NaF), n-Butyl alcohol (n-BuOH) and L-Ascorbic acid (L-AA), were used as the radical scavengers of $^{\bullet}O_2^-$, h^+, and $^{\bullet}OH$, respectively. To identify the dominant active species, scavengers for superoxide radicals, holes and hydroxyl radicals were added to the BB and BG solution before the addition of nanoparticles. In the scavenger experiment, the photodegradation efficiencies were observed as follows: n-BuOH (BB-88%, BG-94%), TBAH (BB-56%, BG-80%), NaF (BB-37%, BG-75%), and L-AA (BB-36%, BG-42%) was found (Fig. 9). This finding suggests that holes and hydroxyl radicals were generated during the photocatalytic degradation process, contributing significantly to the catalyst process. Based on these results, it can be concluded that holes and hydroxyl radicals are the primary active species in this photocatalytic process.

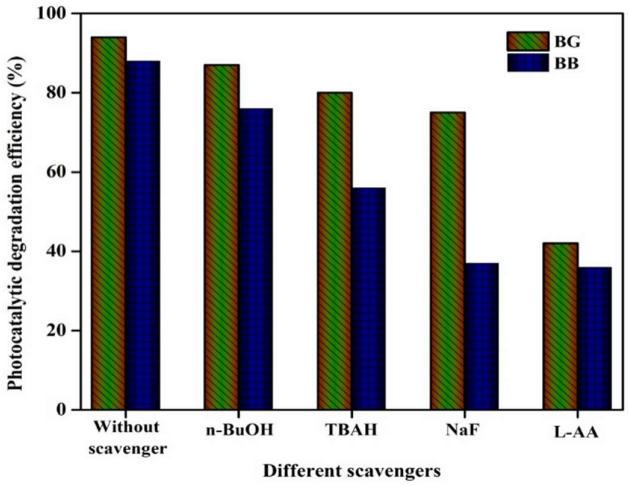

Fig.9 The degradation of BB and BG dyes for Co (0.050 M) doped $PbMoO_4$ catalysts with different scavengers

IV. Conclusion

The synthesized highly efficient bare and Co doped $PbMoO_4$ nanoparticles using the co-precipitation technique and applied them to photodegrade BG and BB as organic contaminants. SEM and HRTEM images reveal a spherical morphology with slight agglomeration. PL emission studies prove that the cobalt doping produces a large number of surface defects/oxygen vacancies in Co (0.050 M) doped $PbMoO_4$. The Co (0.050 M) doped $PbMoO_4$ photocatalyst exhibited superior performance, achieving almost complete degradation rates of 94% for BG and 88% for BB during 120 minutes under visible irradiation. The notable photocatalytic performance of Co (0.050 M) doped $PbMoO_4$ are attributed to the enhanced separation rate of photoexcited charge carriers. Scavenger outcomes suggest that $^{\bullet}OH$ and h^+ play crucial roles in the degradation of BG and BB dyes in the Co (0.050 M) doped $PbMoO_4$ process. The Co doped $PbMoO_4$ catalyst is found to be reusable up to five successive runs. The results showed that the (0.050 M) Co doped $PbMoO_4$ nanoparticles proved to be an efficient photocatalyst for the removal of organic/inorganic pollutants.

Acknowledgements

The authors thank Dr. P. Senthilkumar, Professor of Chemical Engineering and Head, Centre of Excellence in Water Research (CEWAR), Sri Sivasubramaniya Nadar College of Engineering, Kalavakkam, 603 110, Tamil Nadu, India, for providing the experimental facility of all application part, like Photocatalyst, Scavenger studies, COD studies, Catalyst dosage, Reusability measurements.

REFERENCES

[1] H. N. Hamad, & S. Idrus, *Polym.* **14**(4), 783 (2022).

[2] S. Asha, C. Hentry, M. R. Bindhu, A. M. Al-Mohaimeed, M. R. AbdelGawwad, & M. S. Elshikh, *Environ. Res.* **200**, 111721 (2021).

[3] R. Arunadevi, B. Kavitha, R. Karthiga, R., & M. Krishnan, *Asian J. Chem*. **11**(3), 663-670 (2018).

[4] A. Phuruangrat, S. Thongtem, & T. Thongtem, *J. Rare Earths*, **39**(9), 1056-1061, (2021).

[5] A. Mobeen, C. M. Magdalane, S. J. Shahina, D. Lakshmi, R. Sundaram, G. Ramalingam, & K. Kaviyarasu, J. *Surf. Interfac*. **17**, 100381, (2019).

[6] G. Rajesh, P. S. Kumar, G. Rangasamy, S. Akilandeswari, A. Mandal, V. U. Shankar, & K. Thirumalai, *Mol Catal*. **535**, 112835, (2023).

[7] H. Gao, Y. Wang, S. Wang, H. Yang, & Z. Yi, *Solid State Sci.* **129**, 106909, (2022).

[8] C. J. Mao, J. Geng, X. C. Wu, & J. J. Zhu, *J. Phys. Chem. C*. **114**(5), 1982-1988, (2010).

[9] I. Raya, A. A. Mansoor Al Sarraf, G. Widjaja, S. Ghazi Al-Shawi, M. F Ramadan, Z. H. Mahmood, & H. *J. Nanostruct.* **12**(2), 446-454, (2022).

[10] S. K. Ray, D. Dhakal, Y. K. Kshetri, & S. W. Lee, *J. Photochem. Photobiol. A: Chem* **348**, 18-32, (2017).

[11] S. S. Hosseinpour-Mashkani, & A. Sobhani-Nasab, *J. Mater. Sci.: Mater. Electron.* **27**, 4351-4355, (2016).

[12] M. Rajkumar, M. Arunpandian, K. Leeladevi, P. Rameshkumar, & S. Arunachalam, *Phys. B: Condens. Matter*. **620**, 413222, (2021).

[13] M. Bazarganipour, *Ceram. Int.* **42**(11), 12617-12622, (2016).

[14] D. B. Hernández-Uresti, A. Martínez-De La Cruz, & J. A. Aguilar-Garib, J. A. *Catal. today*, **212**, 70-74, (2013).

[15] F. Nobre, J. Trindade, M. do Nascimento, G. Souza, O. Mendes, A. Albuquerque, & J. M. De Matos, *Colorants*, **2**(1), 111-134, (2023).

[16] E. D. O. Gomes, L. Gracia, A. D. A. G. Santiago, R. L. Tranquilin, F. V. D. Motta, R. A. C. Amoresi, & J. Andres, *Phys. Chem. Chem. Phys*. **22**(44), 25876-25891, (2020).

[17] J. Bi, L. Wu, Y. Zhang, Z. Li, J. Li, & X. Fu, *Appl. Catal. B: Environ.* **91**(1-2), 135-143, (2009).

[18] G. Rajesh, P. S. Kumar, S. Akilandeswari, G. Rangasamy, S. Lohita, V. U. Shankar, & K. Thirumalai, *Chemosphere*, **323**, 138232, (2023).

[19] N. A. Neto, L. E. D. Nascimento, M. Correa, F. Bohn, M. R. D. Bomio, & F. V. D. Motta, *Mater. Chem. Phys.* **242**, 122489, (2020).

[20] G. Gyawali, R. Adhikari, B. Joshi, T. H. Kim, V. Rodríguez-González, & S. W. Lee, *J. hazard. mater.* **263**, 45-51, (2013).

[21] J. Zhang, T. Zhao, L. Zou, & S. Gan, *J. Photochem. Photobiol. A: Chem*. **314**, 35-41, (2016).

[22] D. Piwowarska, P. Gnutek, & C. Rudowicz, *Opt. Mater.*, **84**, 466-474, (2018).

[23] G. M. Gurgel, L. X. Lovisa, L. M. Pereira, F. V. D. Motta, M. S. Li, E. Longo, & M. R. D. Bomio, *J. Alloys Compd.* **700**, 130-137, (2017).

[24] J. Zhang, N. Zhang, L. Zou, & S. Gan, *RSC Adv.* **4**(72), 38455-38465, (2014).

[25] T. Skibiński, S. M. Kaczmarek, G. Leniec, T. Tsuboi, Y. Nakai, M. Berkowski, & W. Huang, *J. cryst. growth*, **401**, 802-806, (2014).

[26] R. Lu, J. Luo, X. Wang, A. Chen, Y. Xie, Y. Xu, & Q. Zhan, *Mol. Catal.* **558**, 114033, (2024).

[27] G. Vishnu, S. Singh, T. S. K. Naik, R. Viswanath, P. C. Ramamurthy, P. Bhadrecha, & S. Zahmatkesh, *J. Clean. Prod*. **404**, 136977, (2023).

[28] W. Ahmed, & J. Iqbal, *Ceram. Int.* **46**(16), 25833-25844, (2020).

[29] Z. Chen, Z. He, M. Zhou, M. Xie, T. He, Y. Zhao, & Z. Xu, *Chemosphere*, **284**, 131260, (2021).

[30] F. Lei, B. Yan, H. H. Chen, Q. Zhang, & J. T. Zhao, *Cryst. Growth Des*. **9**(8), 3730-3736, (2009).

[31] V. Q. Hieu, T. K. Phung, T. Q. Nguyen, A. Khan, V. D. Doan, & V. A. Tran, *Chemosphere*, **276**, 130154, (2021).

[32] J. C. Sczancoski, L. S. Cavalcante, N. L. Marana, R. O. da Silva, R. L. Tranquilin, M. R. Joya, & J. Andrés, *Curr. Appl. Phys.* **10**(2), 614-624, (2010).

[33] J. C. Sczancoski, M. D. R. Bomio, L. S. Cavalcante, M. R. Joya, P.S. Pizani, J. A. Varela, & J. A. Andrés, *J. Phys. Chem. C*, **113**(14), 5812-5822, (2009).

[34] R. Nasri, T. Larbi, H. Khemir, M. Amlouk, & M. F. Zid, *Inorg. Chem. Commun.* **119**, 108113, (2020).

[35] J. Guo, C. H. Shen, J. Sun, X. J. Xu, X. Y. Li, Z. H. Fei, & X. J. Wen, *Sep. Purif. Technol.* **259**, 118109, (2021).

[36] B. Zhou, X. Zhao, H. Liu, J. Qu, & C. P. Huang, *Appl. Catal. B: Environ.* **99**(1-2), 214-221, (2010).

[37] C. Y. Wang, Y. J. Zhang, W. K. Wang, D. N. Pei, G. X. Huang, J. J. Chen, & H. Q. Yu, *Appl. Catal. B: Environ.* **221**, 320-328, (2018).

[38] J. Guo, C. H. Shen, J. Sun, X. J. Xu, X. Y. Li, Z. H. Fei, & X. J. Wen, *Sep. Purif. Technol.* **259**, 118109, (2021).

[39] G. Rajesh, P. S. Kumar, S. Akilandeswari, G. Rangasamy, S. Lohita, V. U. Shankar, & K. Thirumalai, *Chemosphere*, **323**, 138232, (2023).

[40] L. Liu, Q. Wei, Y. Lan, & C. Chen, *Chem. Eng. J.* **482**, 149030, (2024).